

Signal-to-Noise Analysis of Cerebral Blood Volume Maps from Dynamic NMR Imaging Studies

Jerrold L. Boxerman, MD, PhD • Bruce R. Rosen, MD, PhD • Robert M. Weisskoff, PhD

The use of cerebral blood volume (CBV) maps generated from dynamic MRI studies tracking the bolus passage of paramagnetic contrast agents strongly depends on the signal-to-noise ratio (SNR) of the maps. The authors present a semianalytic model for the noise in CBV maps and introduce analytic and Monte Carlo techniques for determining the effect of experimental parameters and processing strategies upon CBV-SNR. CBV-SNR increases as more points are used to estimate the baseline signal level. For typical injections, maps made with 10 baseline points have 34% more noise than those made with 50 baseline points. For a given peak percentage signal drop, an optimum TE can be chosen that, in general, is less than the baseline T2. However, because CBV-SNR is relatively insensitive to TE around this optimum value, choosing TE \approx T2 does not sacrifice much SNR for typical doses of contrast agent. The TR that maximizes spin-echo CBV-SNR satisfies TR/T1 \approx 1.26, whereas as short a TR as possible should be used to maximize gradient-echo CBV-SNR. In general, CBV-SNR is maximized for a given dose of contrast agent by selecting as short an input bolus duration as possible. For image SNR exceeding 20–30, the Γ -fitting procedure adds little extra noise compared with simple numeric integration. However, for noisier input images, as can be the case for high resolution echo-planar images, the covarying parameters of the Γ -variate fit broaden the distribution of the CBV estimate and thereby decrease CBV-SNR. The authors compared the analytic noise predicted by their model with that of actual patient data and found that the analytic model accounts for roughly 70% of the measured variability of CBV within white matter regions of interest.

Index terms: Cerebral blood volume mapping • Signal-to-noise ratio • Monte Carlo modeling • Optimization of imaging parameters

From the MGH-NMR Center, Massachusetts General Hospital, Department of Radiology, and Harvard Medical School, Building 149 (2301), 13th Street, Charlestown, MA 02129. Received November 12, 1996; revision requested December 30; revision received January 16, 1997; accepted January 17. This work was supported in part by National Institutes of Health Grants P01-48729 and R01-HL39810, a grant from the Whitaker Foundation, and a Clement Vaturi Fellowship. Results presented herein were presented at the annual scientific meeting of the Society of Magnetic Resonance in Medicine, Berlin, 1992. Current affiliation for J.L.B.: Department of Radiology and Radiological Science, The Johns Hopkins University School of Medicine, Baltimore, MD. Address reprint requests to R.M.W.

© ISMRM, 1997

JMRI 1997; 7:528–537

Abbreviations: CBV = cerebral blood volume, Dy-DTPA = dysprosium-diethylenetriamine pentaacetic acid, 18 FDG = flurodeoxyglucose, Gd-DTPA = gadolinium-diethylenetriamine pentaacetic acid, MTT = mean transit time, PET = positron emission tomography, ROI = region of interest, SNR = signal-to-noise ratio.

DYNAMIC MRI STUDIES tracking both gadolinium-diethylenetriamine pentaacetic acid (Gd-DTPA) (1–3) and dysprosium-diethylenetriamine pentaacetic acid (Dy-DTPA) (4) have produced MR cerebral blood volume (CBV) maps. Such susceptibility contrast-based CBV maps have been used to study normal human brain task activation (5–7) and to evaluate patients with brain tumors (2,8) and are therefore becoming important for both understanding fundamental questions of neuroscience and also for improving diagnostic sensitivity and specificity in various neuropathologies. MR CBV maps seem to correlate closely to tumor grade, match positron emission tomography (PET) flurodeoxyglucose (18 FDG) maps in most cases studied, may have an important role in guiding tumor biopsy, and may help to differentiate recurrent tumor from radiation necrosis (9–11).

The use of CBV maps strongly depends on the signal-to-noise ratio (SNR) of the maps. In this paper, we produced a semianalytic model that characterizes the main sources of noise in computed CBV maps. This model was used in conjunction with Monte Carlo techniques to evaluate the effects of the following imaging parameters on CBV-SNR: estimation of the baseline signal, choice of TE and peak signal drop, choice of TR, duration of the bolus of contrast agent, and effects of Γ -variate fitting (12,13) to the signal-time curve. Where appropriate, we used Monte Carlo methods to validate the model. To assess the validity of the model, we compared the analytic noise predicted by our model with an estimate from gray and white matter regions of interest (ROIs) from actual patient data.

• CBV MAP THEORY

From elementary tracer kinetics (14), the area under the tissue concentration-time curve for a purely intravascular tracer is proportional to local blood volume. In the presence of an intact blood-brain barrier, Gd-DTPA and Dy-DTPA remain intravascular during cerebral passage, and hence the associated concentration-time curve can

be processed to compute CBV. Both experimental data (15) and Monte Carlo modeling (16) have demonstrated a relatively linear relationship between the tissue concentration of contrast agent and transverse relaxivity change, $\Delta R2^* = \Delta(1/T2^*)$ and $\Delta R2 = \Delta(1/T2)$. Furthermore, in many cases, correct relative comparisons of CBV can be made even with a nonlinear concentration dependence. (16) We therefore obtain a first-order relative CBV estimate, V , for a voxel by integrating $\Delta R2(t)$ without concern for the arterial concentration-time data or the proportionality factor-relating agent concentration to $\Delta R2^*$ or $\Delta R2$.

As an approximation of the area under the concentration-time curve, the CBV map that we frequently create is a simple numeric integration of the $\Delta R2$ -time curve across a time interval chosen to eliminate the effects of contrast agent recirculation:

$$V = TR \sum_{i=1}^N \Delta R2_i = -\frac{TR}{TE} \sum_{i=1}^N \ln \left(\frac{S_i}{S_o} \right), \quad (1)$$

where

$$\Delta R2_i = -\frac{1}{TE} \ln \left(\frac{S_i}{S_o} \right) \quad (2)$$

converts signal magnitude changes on the MR images into approximate transverse relaxivity change. S_i is the MR signal intensity at time point i , N is the number of time points used for the integration, TR is the time spacing between echo-planar or fast-gradient-echo acquisitions, and

$$S_o = \frac{1}{N_b} \sum_{j=1}^{N_b} S_j \quad (3)$$

is an estimate of the signal, before injection of contrast agent, calculated from N_b baseline images. We produce a CBV map by calculating V for each voxel within an ROI.

When recirculation of contrast agent is significant, Γ -variate fits to $\Delta R2(t)$ of the form

$$\Delta R2(t) = K (t - t_o)^\alpha e^{-(t - t_o)/\beta} \quad (4)$$

have been used to eliminate second-pass effects (5,17). The area under the first-pass $\Delta R2(t)$ curve is estimated by

$$V = K \cdot \Gamma(1 + \alpha) \cdot \beta^{1 + \alpha}, \quad (5)$$

where $\Gamma(x)$ is the Γ -variate function (18). Integrating the resulting Γ -variate curve may provide a more accurate estimate of V , because recirculation artificially elevates estimates of CBV, and simple numeric integration of $\Delta R2$, with a cutoff before the onset of recirculation probably underestimates CBV.

• METHODS

Analytic Error Analysis

To assess the statistic error in the computed estimate of CBV, σ_v , we first propagate the errors, assuming that the underlying MR image set has noise σ_o . Combining Equations [1] and [3] yields:

$$V = -\frac{TR}{TE} \sum_{i=1}^N \ln(S_i) + \frac{NTR}{TE} \ln \left(\frac{1}{N_b} \sum_{j=1}^{N_b} S_j \right). \quad (6)$$

Assuming that the noise is white, so that the fluctuations in S_i and S_j are uncorrelated, we find that σ_v can be approximated by (19):

$$\begin{aligned} \sigma_v^2 &= \sigma_o^2 \sum_{i=1}^N \left(\frac{\partial V}{\partial S_i} \right)^2 + \sigma_o^2 \sum_{j=1}^{N_b} \left(\frac{\partial V}{\partial S_j} \right)^2 \\ &= \frac{\sigma_o^2 N TR^2}{TE^2 S_o^2} \left(\zeta + \frac{N}{N_b} \right), \end{aligned} \quad (7)$$

where

$$\zeta = \frac{S_o^2}{N} \sum_{i=1}^N \frac{1}{S_i^2} \quad (8)$$

is a numeric factor of order unity that incorporates noise due to logarithm calculation. Therefore, σ_v has two terms: one due specifically to the variance of the integrated $\Delta R2(t)$ images, and one due to the estimate of the baseline, S_o (20). A semianalytic estimate of SNR is obtained by dividing V in Equation [6] by σ_v in Equation [7].

For a more intuitive appreciation for CBV-SNR, the area under $\Delta R2(t)$ can be expressed as:

$$V = \frac{AN_{fwhm}TR}{TE} \ln \left(\frac{S_o}{S_{min}} \right), \quad (9)$$

where N_{fwhm} is the number of images across the half-maximum point of $\Delta R2(t)$, S_{min} is the minimum signal intensity during passage of the contrast agent bolus, and A is a numeric factor of order unity that makes the area under $\Delta R2(t)$ is correct. Dividing Equation [9] by σ_v yields:

$$SNR = \frac{V}{\sigma_v} = SNR_o \frac{AN_{fwhm} \ln(S_o/S_{min})}{\sqrt{N} (\zeta + N/N_b)}, \quad (10)$$

where SNR_o equals S_o/σ_o . CBV-SNR equals SNR_o scaled by a factor proportional to the width and peak of $\Delta R2(t)$ and inversely related to a noise term including the number of integration points, the variance of the integrated images, and the number of baseline points.

Monte Carlo Error Analysis

We used Monte Carlo techniques to quantify the effects of nonlinear, Γ -variate fits to $\Delta R2(t)$ described in Equation [4]. We also used a Monte Carlo approach to simulate variation in sampling offset relative to the onset of the contrast agent bolus. For large TR , varied sampling offset influences the characterization of $\Delta R2(t)$ and therefore introduces variance in V . Varied sampling offset also introduces variance in V through the numeric integration process itself, regardless of the sampling rate. Propagation of errors is untenable for these nonlinear effects.

To obtain a Monte Carlo CBV estimate (18), zero-mean Gaussian noise with signal-domain variance σ^2 was added to the parent data described below to generate 10^4 synthetic data sets with input signal $SNR = S_o/\sigma$. This noise was added to the parent signal domain data using variance σ^2 for each data point, and S_o was re-estimated to convert the signal data to the $\Delta R2$ domain. Although it oversimplifies the Ricean noise in the MR images, this Gaussian assumption is nevertheless a good approximation for $SNR > 5$, which was satisfied by all of our simulations.

Sampling offset was included for each synthetic data set by randomly selecting a starting time point uniformly distributed between $\pm TR/2$ of the input starting time point, regenerating the parent curves using the parent Γ -variate parameters at successive TR intervals, and then adding the appropriate noise. The CBV for each synthetic data set was then computed either numerically using Equation [1] or via a Γ -variate fit using Equations [4] and [5]. Numeric integration employed the extended trapezoidal rule (18) with initial and terminal zero-padding over a range delineated by the times at which the parent

$\Delta R2(t)$ curve first rose above and then fell below one σ . For Γ -variate fitting, we used a modified simplex algorithm (18) that minimized weighted χ^2 error for the four-parameter fit in Equation [4]. A 51-bin histogram of the resulting CBV values from the 10^4 trials was then constructed. The "signal" of the CBV estimate was defined to be the mean of the computed V values for all of the synthetic data sets. The "noise" of the CBV estimate was defined to be one-half of the 66% confidence interval of the CBV histogram.

Human Data

We first acquired images using a fat-suppressed, spin-echo echo-planar imaging (EPI) pulse sequence with TE = .1 second and TR = 1.0 second, as described by Aronen et al (10). A total of 120 axial images with a slice thickness of 7 mm and an in-plane resolution of 1.5×1.5 mm were acquired at 1.0-second intervals before, during, and after antecubital power-injection (Medrad, Pittsburgh, PA) of a 30-cc, .2-mmol/kg dose of Omniscan (Gadodiamide [Gd-DTPA-BMA], Nycomed, New York, NY) at an injection rate of 5.0 ml/second. Each image was smoothed spatially with a 3×3 Hanning filter. A sample pixel was selected from a gray matter ROI for which it was assumed for purposes of the simulations that T1 = .8 second and T2 = .1 second. The first $N_b = 60$ baseline images of the remaining time series data were used to estimate both the baseline, S_o , and the variance of the background image signal intensity, σ_v^2 , for the sample pixel. The sample signal data were converted to $\Delta R2_i$ data via Equation [2]. The $\Delta R2_i$ data were then fit to a Γ -variate function, which was resampled at TR, thereby yielding parent $\Delta R2$ data. Parent signal data were then obtained from the parent $\Delta R2$ data using Equation [2].

Signal Baseline Estimation

Equation [7] relates the number of baseline images, N_b , to σ_v neglecting sampling effects. The fraction of σ_v due to signal baseline estimation was calculated by comparing σ_v for N_b ranging from 0 to 100 with σ_v for $N_b \rightarrow \infty$. $N = 15$ (typical for TR = 1 second) and $\zeta = 1.0, 1.2$ (the value for our sample data), 2.0, and 3.0 were chosen. A Monte Carlo estimate of σ_v for N_b ranging from 3 to 60, stepping by 3, also was performed and compared with a Monte Carlo estimate of σ_v , for which noise was added directly to $\Delta R2$ without re-estimation of baseline ($N_b \rightarrow \infty$). The Monte Carlo noise fraction estimate was compared with the analytic estimate for $\zeta = 1.2$. In each simulation, identical input signal noise, σ_o , was added, but S_o was re-estimated for each N_b . We also used the Monte Carlo technique on the parent data to produce CBV-SNR versus input-SNR curves for $\zeta = 1.2, N = 15$, and $N_b = 2, 10, 60$, and ∞ . The range of input noise was chosen to yield an input image SNR range of 10 to 1,000.

Choice of TE and Peak Signal Drop

To determine the TE that maximizes CBV-SNR, we propagated errors for $\Delta R2_i$, as in Equations [6] and [7] using

$$S_i \sim (1 - e^{-TR/T1})e^{-TE/T2} = (1 - e^{-TR/T1})e^{-TE(R2_o + \Delta R2_i)} \quad (11)$$

for a spin-echo sequence (with TE \ll 2T1), and

$$S_i \sim \tan\left(\frac{\theta}{2}\right)e^{TE/T2^*} = \tan\left(\frac{\theta}{2}\right)e^{-TE(R2_o^* + \Delta R2_i^*)} \quad (12)$$

for a spoiled gradient-echo sequence acquired at the Ernst angle, $\theta = \cos^{-1}(e^{-TR/T1})$. We then set the derivative of the noise with respect to TE = 0 and solved for TE.

To test the derived analytic relationships, we generated synthetic data sets with maximum signal drops of 10%, 30%, 50%, 70%, and 90% of baseline S_o from the parent data set. Scaled signal curves with TE ranging from 20 to 160 msec with an increment of 2 msec were then generated for each maximum signal drop. First, the original signal data, S_i , with baseline S_o were appropriately scaled to simulate the tissue response, also with baseline S_o , to a contrast agent dose yielding the desired maximum signal drops. Next, the transformed data were further scaled by an exponential factor to properly account for the signal attenuation imposed by each desired TE. This second transformation preserved the peak signal drop resulting from the first transformation; only the signal data were modified. These transformations assumed a linear mono-exponential relationship between contrast agent concentration and signal loss.

For each generated signal curve, both a Monte Carlo estimate and a semianalytic estimate of CBV-SNR were obtained with noise σ_o added to the signal domain. The appropriate ζ for the peak $\Delta R2$ was calculated directly from the S_i and S_o at the original TE using Equation [8], and this ζ was used in the analytic estimate. For each parent data set for a given peak percentage signal drop, the optimum TE was estimated as described above and compared with the TE yielding maximum Monte Carlo and analytic CBV-SNR.

Choice of TR

To determine the TR that maximizes CBV-SNR, we propagated errors for $\Delta R2_i$ using Equation [11] for a spin-echo signal and Equation [12] for a gradient-echo signal. We then set the derivative of the noise with respect to TR = 0 and solved for TR for both the spin-echo and gradient-echo signals.

To test the derived relationships and to consider the effects of undersampling and variation of sampling times, synthetic spin-echo and gradient-echo data sets were generated from the parent data set with TR ranging from 150 msec (1.5 TE) to 3.0 seconds with an increment of 20 msec and TE constant at 100 msec. To simulate data sets acquired at various TRs from the parent data set, S_i , we started at the initial baseline time point and sampled the parent $\Delta R2_i$ every TR using the Γ -variate parameters to generate intermediate $\Delta R2$ values. Sample time variation was simulated by randomly selecting the initial sample point, as described above. We next appropriately scaled the resampled signal by a scaling factor chosen to account for the relative signal attenuation between data acquired at various TRs. For each transformed signal curve, a Monte Carlo CBV-SNR estimate, with and without the effects of sample variation, in addition to an analytic estimate of CBV-SNR were performed. The TR at which the Monte Carlo and analytic SNR peaked were compared with the predicted optimum TR.

Contrast Agent Bolus Duration

To determine the effect of contrast agent bolus duration on CBV-SNR, the β and K parameters of the parent Γ -function (Equation [4]) were adjusted, keeping the area, $K\beta^{(1+\alpha)}$, constant. This produced multiple $\Delta R2(t)$ curves with constant area, V_o , and various first moments, thereby simulating tissue responses to input boluses of various duration but constant dose of contrast agent. Because the mean transit time (MTT) of the tissue response equals the sum of the MTT of the input bolus and the MTT of the tissue impulse function, the MTT of the tissue response directly reflects the MTT (and hence the duration) of the input bolus. The rise parameter, α , was fixed

at $\alpha = 1$, and t_0 was set at zero with no loss of generality. For each simulated tissue response curve, $\Delta R2(t)$, the optimum TE was estimated as above, and the signal data were scaled as described above to optimize CBV-SNR with respect to TE. Each TE-optimized $\Delta R2$ curve was resampled at TR = .5, 1.0, and 1.5 seconds, and sample offset was included to simulate the effects of sampling variation. Both analytic and Monte Carlo CBV-SNR estimation, using numeric integration and time-domain noise σ_v equal to that of the sample data, were performed for each adjusted β and K pair as a function of tissue response transit time for each TR.

Γ -Variate Fitting

Using the Monte Carlo technique, we assessed the amount of noise added to the map generation process by estimating V with a Γ -variate fit instead of numeric integration. From the parent data, CBV-SNR versus input SNR curves were obtained for $N_b = 30$ using both numeric integration and Γ -variate fitting, and these curves were compared to assess the amount of additional noise introduced by the Γ -variate fit.

Comparison of Model with Clinical Data

We compared the analytic noise, σ_v , predicted by our model (Equation [7]) with that of clinical CBV maps. For each of $n = 7$ patients, we obtained a high resolution T1-weighted image for differentiating gray and white matter. We then obtained a series of spin-echo images during first passage of a bolus injection of Gd-DTPA as described above. Each image in the time series was then smoothed with a 3×3 Hanning filter. For each voxel, S_0 was estimated from the baseline of the corresponding time series (Equation [3], $N_b = 60$ points), and $S(t)$ was converted to $\Delta R2(t)$ via Equation [2]. Relative CBV maps of V were constructed by numerically integrating $\Delta R2(t)$ over $N = 16$ points covering the duration of bolus.

We next made an analytic estimate of σ_v . Sample-smoothed time course data were obtained from one voxel in a white matter ROI (8×8 voxels) chosen from the T1-weighted image. We calculated σ_v and S_0 from N_b baseline points, and we calculated ζ from N bolus points. An analytic estimate of σ_v was then obtained using Equation [7].

We obtained an experimental estimate of σ_v by dividing the 8×8 pixel ROI into 2-pixel, nonoverlapping sub-ROIs. We computed the standard deviation of V within each sub-ROI and averaged these 32 standard deviations to estimate σ_v in the white matter. This reduces the effects of the actual variation in true blood volume found within the 8×8 pixel ROI. To the extent that neighboring pixels reflect similar tissue with equal V , the average standard deviation of the sub-ROIs reflects the repeatability of CBV measurements and is an estimate of σ_v . (This estimate of the variance is analogous to the Allan variance used to characterize the fluctuations in atomic clocks [21]). We then computed the mean and standard deviation of the average sub-ROI standard deviation for all $n = 7$ patients. We also repeated this analysis for 4-pixel (2×2) sub-ROIs and repeated the 2- and 4-pixel sub-ROI analysis for a 8×8 gray matter ROI. Because the pixels were smoothed spatially before constructing these maps, the average standard deviation of the sub-ROIs was multiplied by a factor accounting for both the correlation introduced by the Hanning filter and the correlation introduced by the size of the sub-ROI (2.4 for 2-pixel sub-ROIs and 1.8 for 4-pixel sub-ROIs; see Appendix). We then compared the analytic with the experimental σ_v .

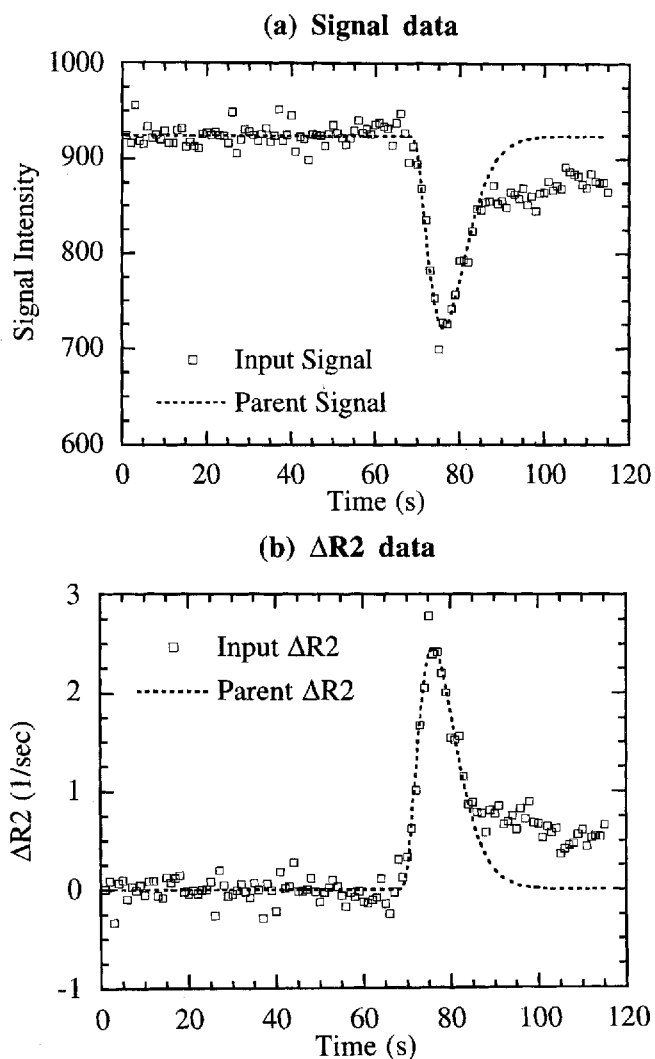


Figure 1. (a) The sample and parent signal data with $S_0 = 924$, $\sigma_v = 11$, and $\zeta = 1.2$. (b) The sample and parent $\Delta R2$ data. The derived Γ -fit parameters for 15 data points between $t = 65$ seconds and $t = 80$ seconds are $K = .1$, $t_0 = 68.4$, $\alpha = 3.2$, and $\beta = 2.4$, corresponding to an area V_0 of 24.1 ($\Delta R2$ units).

• RESULTS

Human Data

Typical sample and parent signal data are shown in Figure 1a, and the corresponding $\Delta R2$ data are shown in Figure 1b. For the sample input data, $S_0 = 924$ and $\sigma_v = 11$. The input $\Delta R2$ data were fit to a Γ -function between $t = 65$ seconds and $t = 80$ seconds ($N = 15$ data points). Over this range, ζ (Equation [8]) was found to be 1.2. The derived Γ -fit parameters were $K = .1$, $t_0 = 68.4$ seconds, $\alpha = 3.2$, and $\beta = 2.4$ seconds, corresponding to an area V_0 of 24.1 ($\Delta R2$ units).

Signal Baseline Estimation

The fraction of total CBV map noise due to baseline estimation, η_b , was found to be:

$$\eta_b = \frac{\sigma_v - \sigma_{v, N_b \rightarrow \infty}}{\sigma_v} = 1 - \sqrt{\frac{\zeta}{\zeta + N/N_b}} \quad (13)$$

In Figure 2a, η_b is plotted as a function of N_b for $N = 15$. For $\zeta = 1.2$, roughly 50 baseline images would be required to reduce the baseline contribution to 10% of the total CBV map noise. By comparison, maps for which $\zeta = 1.2$ and $N_b = 10$ images have 34% more noise. It is also

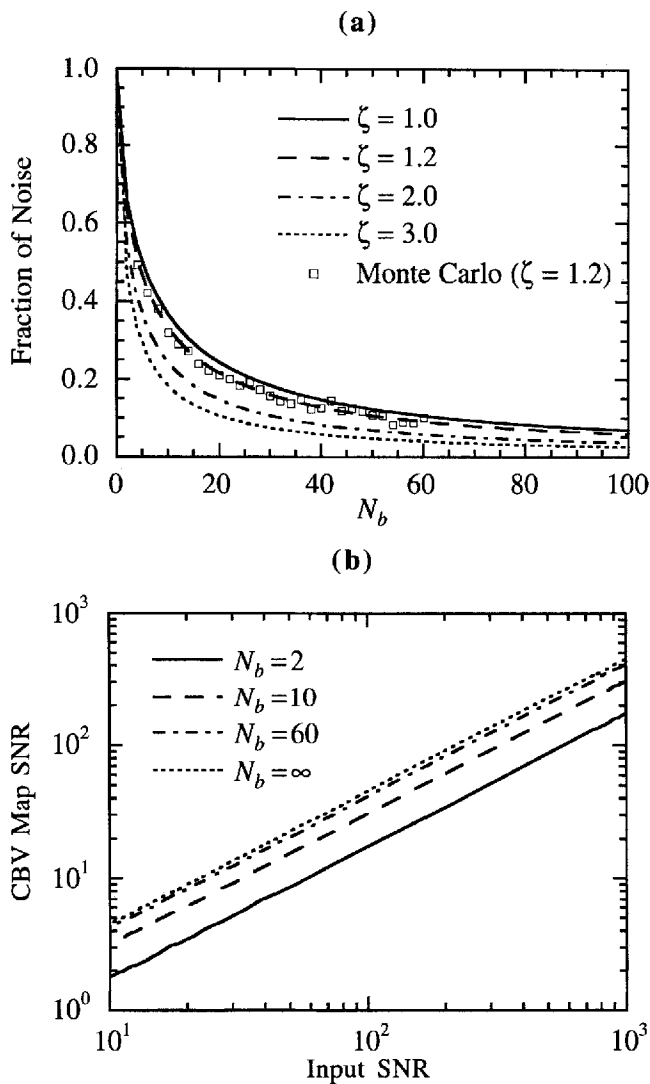


Figure 2. (a) Fraction of noise, η_b , plotted as a function of N_b for $N = 15$ and $\zeta = 1.0, 1.2, 2.0,$ and 3.0 . For $\zeta = 1.2$, roughly 50 baseline images would be required to reduce the baseline contribution to 10% of the total CBV map noise. As ζ increases, the baseline estimate becomes less significant. The Monte Carlo estimates of η_b (□) for $\zeta = 1.2$ and $N = 15$ agree well with the analytic estimates for the sample data. (b) Input SNR plotted against Monte Carlo CBV-SNR. With increasing N_b , the SNR curves asymptotically approach the $N_b \rightarrow \infty$ curve in which baseline noise is excluded.

evident that as ζ increases, baseline estimate becomes less significant. The Monte Carlo estimates of η_b (square symbols) are compared with the analytic estimates for the sample data ($\zeta = 1.2, N = 15$), and excellent agreement is observed. In Figure 2b, input SNR is plotted against Monte Carlo CBV-SNR. With increasing N_b , the SNR curves asymptotically approach the $N_b \rightarrow \infty$ curve in which baseline noise is excluded.

Choice of TE and Peak Signal Drop

From propagation of errors in Equation [2], the error for the i th $\Delta R2$ (and $\Delta R2^*$) value, σ_i , in terms of input noise, σ_o , and signal value, S_i , is:

$$\sigma_i = \frac{\sigma_o}{TE S_i} = \frac{\sigma_o}{TE f(TR, T1)} e^{TE(R2_o + \Delta R2_i)}, \quad (14)$$

where f is a function of TR and T1 only and sampling effects have been omitted. By minimizing total noise,

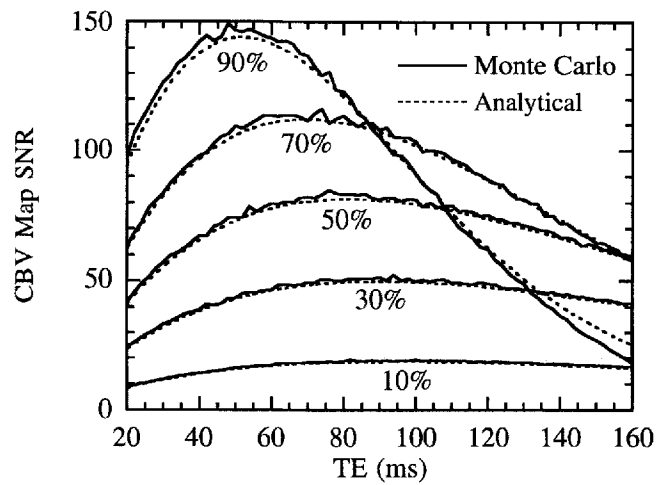


Figure 3. Effect of TE and peak signal drop on CBV-SNR. Analytic and Monte Carlo CBV-SNR are plotted against TE for peak signal drops of 10%, 30%, 50%, 70%, and 90%. The analytic and Monte Carlo results agree exceptionally well. Because constant signal domain noise σ_o is added to each curve, peak SNR increases with increasing peak $\Delta R2$, because V/σ_o increases. As peak $\Delta R2$ increases, TE_{opt} decreases. Given a peak signal drop and a particular shape of $\Delta R2(t)$, an optimum TE can be chosen.

$$\sigma_v^2 = TR^2 \sum_{i=1}^N \sigma_i^2, \quad (15)$$

with respect to TE, we find that the TE that maximizes CBV-SNR, TE_{opt} , must satisfy:

$$\sum_{i=1}^N (R2_o + \Delta R2_i - \frac{1}{TE_{opt}} e^{zTE_{opt} \Delta R2_i}) = 0, \quad (16)$$

with $T2_o = 1/R2_o$. We solved Equation [16] numerically for TE_{opt} . When $\Delta R2_i \ll R2_o$, then $TE_{opt} = T2$, as expected.

In Figure 3, the analytic and Monte Carlo CBV-SNR results are plotted against TE for each peak signal drop, and excellent agreement is observed. Because constant signal-domain noise, σ_o , is added to each curve, peak SNR increases with increasing peak $\Delta R2$, because V/σ_o increases. Furthermore, as peak $\Delta R2$ increases, TE_{opt} decreases, which is predicted by Equation [16].

Choice of TR

For a spin-echo sequence, neglecting undersampling, we propagated errors using Equations [11] and [14] and proceeded as we did in Equation [15] using:

$$TR \sum_{i=1}^N e^{2 TE \Delta R2_i} \approx C, \quad (17)$$

where C is independent of TR and is strictly a function of the $\Delta R2$ curve. We obtained:

$$\sigma_v^2 \sim \frac{\sigma_o^2 C e^{2 TE R2_o}}{TE^2} \cdot \frac{TR}{(1 - e^{-TR/T1})^2}, \quad (18)$$

The TR that minimizes σ_v , TR_{opt} , should maximize CBV-SNR and must satisfy:

$$\frac{2 TR_{opt}/T1}{e^{TR_{opt}/T1} - 1} = 1, \quad (19)$$

which can be solved numerically to yield:

$$\frac{TR_{opt}}{T1} \approx 1.26. \quad (20)$$

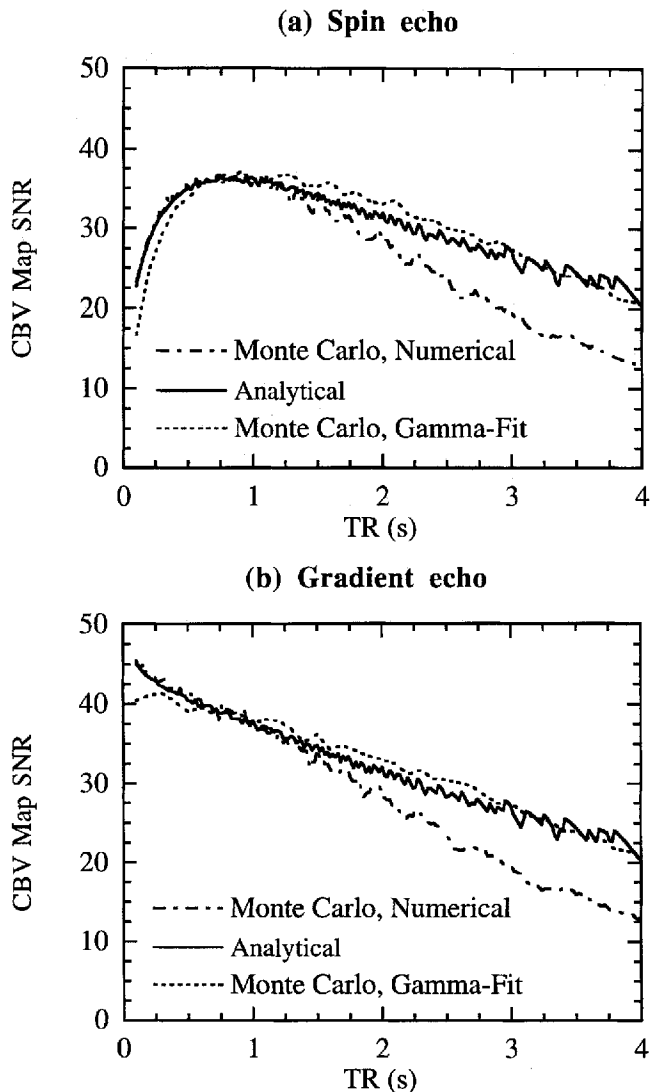


Figure 4. Effect of TR on CBV-SNR. Monte Carlo and analytic CBV-SNR plotted against TR for (a) spin-echo and (b) gradient-echo acquisitions. TR ranges from 150 msec (1.5 TE) to 3.0 seconds. For the spin-echo simulation, CBV-SNR peaks at TR = 1.0 second $\approx 1.25 T_1$ in the absence of sample offset variation. For the gradient-echo simulation, CBV-SNR monotonically decreases with TR.

The TR that optimizes CBV-SNR when undersampling is neglected is strictly a function of tissue T_1 and is independent of the shape of the bolus, at least in the limit that fluctuations in the initial timing of the bolus can be neglected.

Proceeding along similar lines for a spoiled gradient-echo sequence using Equations [12] and [14]:

$$\sigma_v^2 \sim \frac{\sigma_o^2 C e^{2 TE R_2}}{TE^2} \cdot \frac{TR (1 + e^{-TR/T_1})}{1 - e^{-TR/T_1}}. \quad (21)$$

Solving $\partial\sigma_v^2/\partial TR = 0$ yields:

$$\frac{TR_{opt}}{T_1} = 0. \quad (22)$$

Therefore, we should use as short a TR as possible to optimize gradient-echo CBV-SNR.

Monte Carlo and analytic CBV-SNR are plotted against TR for spin-echo acquisitions in Figure 4a and for gradient-echo acquisitions in Figure 4b. For the spin-echo simulation, CBV-SNR peaks at TR = 1.0 second ≈ 1.25

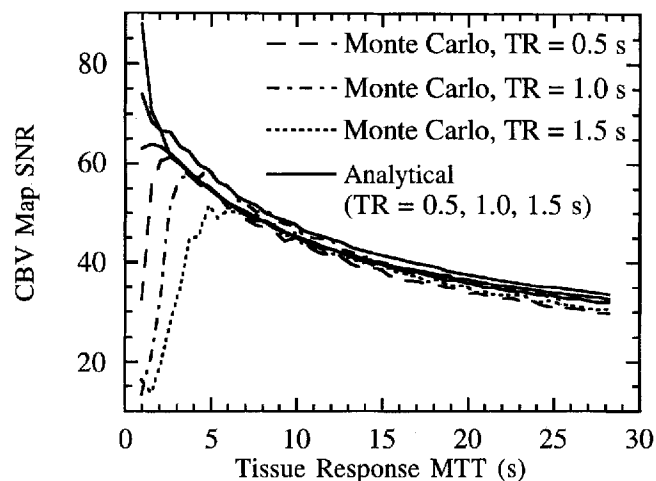


Figure 5. Effect of input bolus duration as reflected by tissue response MTT on CBV-SNR. CBV-SNR for a given contrast agent dose is maximized by selecting as short an input bolus duration as possible. For sufficiently short TR such that $\Delta R_2(t)$ is sampled adequately, CBV-SNR versus tissue response transit time is independent of TR. The decrease in Monte Carlo CBV-SNR for short tissue response MTT reflects the inability of the numeric integration scheme to precisely integrate $\Delta R_2(t)$ when the input time is unknown. This effect becomes increasingly more pronounced with increasing TR, because $\Delta R_2(t)$ is more coarsely sampled.

T_1 , which agrees with Equation [20]. For the gradient echo simulation, CBV-SNR monotonically decreases with TR, which supports Equation [22].

Contrast Agent Bolus Duration

Figure 5 shows plots of analytic and Monte Carlo (numeric integration) CBV-SNR as a function of the MTT of the tissue response with TE_{opt} chosen for each $\Delta R_2(t)$ curve. To the extent that the tissue response transit time reflects input bolus duration, Figure 5 demonstrates that over a range of physiologic bolus durations, we maximize CBV-SNR for a given contrast agent dose by selecting as short an input bolus duration as possible. For sufficiently short TR such that $\Delta R_2(t)$ is adequately sampled, CBV-SNR versus tissue response transit time is independent of TR.

Γ -Variate Fitting

Figure 6 plots CBV-SNR versus input SNR curves for $N_b = 30$ using numeric integration and Γ -variate fitting. For input image SNR exceeding 20 to 30, the Γ -fitting procedure adds little extra noise compared with simple integration. However, for noisier input images, the co-varying parameters of the Γ -variate fit process broaden the distribution of the blood volume estimate, V , and thereby decrease the CBV-SNR. This threshold was observed consistently across the sampled patient data.

Comparison of Model with Clinical Data

Table 1 summarizes the comparison of the analytic model of σ_v with the experimental variability of CBV. The mean and standard deviations of the average sub-ROI standard deviations for all $n = 7$ subjects are tabulated for both the 2- and 4-pixel sub-ROIs and for both gray and white matter. The 2- and 4-pixel "adjusted" columns include the factor accounting for Hanning filter and sub-ROI correlation. Also tabulated are the mean and standard deviation of analytic σ_v for all $n = 7$ patients. Because V is dimensionless and independent of receiver

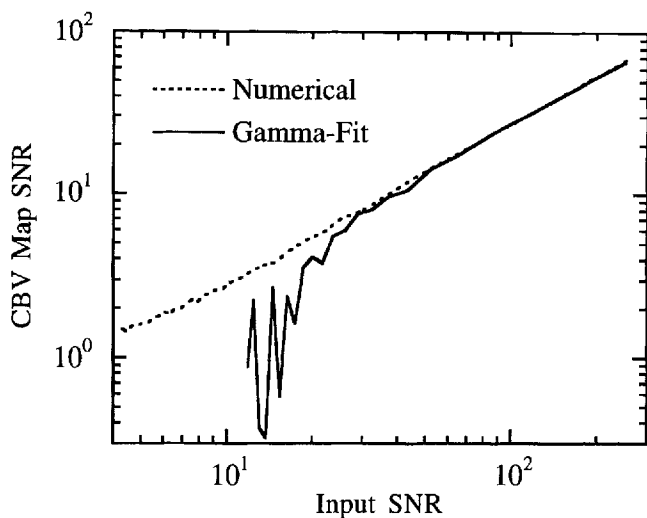


Figure 6. Effect of Γ -variate fitting on CBV-SNR. Monte Carlo CBV-SNR is plotted against input SNR for $N_b = 30$ using numeric integration and Γ -variate fitting. For input image SNR exceeding 20 to 30, the Γ -fitting procedure adds little extra noise compared with simple integration. However, for noisier input images, the covarying parameters of the Γ -variate fit process broaden the distribution of the blood volume estimate, V , and thereby decrease the CBV-SNR.

gain, the entries in Table 1 are unitless. For gray matter, the analytic σ_v accounts for 56% and 49% of the 2- and 4-pixel adjusted noises, respectively. For white matter, however, the analytic σ_v is much closer to experimental variability and accounts for roughly 70% and 61% of the 2- and 4-pixel adjusted noises, respectively.

• DISCUSSION

This study characterizes the main sources of noise in computed CBV maps and determines the experimental parameters and processing strategies that maximize CBV-SNR. This work focuses on the noise introduced in the map generation process itself and does not consider those factors that influence σ_v , such as inherent imaging system noise and temporal physiologic variations. We propagated errors for a simple expression of calculated CBV, the numeric integration of $\Delta R2(t)$ over a time interval covering only the first-pass bolus response. Alternative methods to compute relative CBV have been employed, including numeric integration over the entire $\Delta R2(t)$ response, integration over the Γ -variate fit (7,8), selection of the peak $\Delta R2$ (6), and techniques that work directly in the signal domain without conversion to $\Delta R2$ (22). Equation [7] suggests that integration over the entire $\Delta R2(t)$ response adds considerable noise to the CBV maps, because N is large in such cases, and σ_v increases with N even if the number of points used for baseline estimation, N_b , is substantial. To minimize CBV map noise but maintain fair comparisons of relative CBV, N should be chosen to be no larger than is necessary to entirely cover the duration of the first-pass bolus. As depicted in Figure 6, Γ -variate fits do not contribute additional CBV map noise if the input SNR is sufficiently large to eliminate the variability introduced by the covarying parameters of the fit. As the input data become noisier, this variability worsens, and Γ -variate fits yield decreased CBV-SNR. In practice, we typically obtain high resolution CBV maps (to see increasingly small structures) so that the underlying functionally weighted images often are near or below this SNR limit. Selecting the peak $\Delta R2$ is

Table 1
Comparison of Analytical and Experimental CBV Map Noise

| | 2-pixel | 2-pixel Adjusted | 4-pixel | 4-pixel Adjusted | Analytic |
|-------|--------------|------------------|--------------|------------------|--------------|
| White | $1.2 \pm .3$ | $2.9 \pm .7$ | $1.8 \pm .4$ | $3.3 \pm .8$ | $2.0 \pm .4$ |
| Gray | $2.0 \pm .5$ | 4.8 ± 1.2 | $3.1 \pm .8$ | 5.5 ± 1.4 | $2.7 \pm .7$ |

Note.—Comparison of the analytic model of σ_v with the experimental variability of CBV. The mean and standard deviations of the average sub-ROI standard deviations for $n = 7$ subjects are tabulated for 2- and 4-pixel sub-ROIs and for gray and white matter. The "adjusted" columns include the factor accounting for Hanning filter and sub-ROI correlation. Also tabulated are the mean and SD of analytic σ_v for all $n = 7$ subjects. For gray matter, the analytical σ_v accounts for 57% and 49% of the 2- and 4-pixel adjusted noises, respectively. For white matter, however, the analytical σ_v is much closer to experimental variability and accounts for 70% and 61% of the 2- and 4-pixel adjusted noises, respectively.

suboptimal because the peak is not always directly proportional to the area under $\Delta R2(t)$. In the single-step method introduced by Bahn (22), CBV as well as S_0 are parameters in a model fit directly to the original S_t data, thereby eliminating the log and baseline components of our model for σ_v . Although it remains to be shown how the propagation of noise in the multiparameter fit of the single-step method compares with the noise introduced by baseline estimation and logarithm calculation in the numeric integration technique, it is reasonable to expect that our predictions could be used, with the noise behaving as if all of the points ($N_b + N$) were used for the baseline estimation.

For the current methods, baseline estimation strongly influences CBV-SNR. Figure 2b demonstrates that for $\zeta = 1.2$ and $N = 15$, $N_b = 60$ and $N_b = 50$ baseline points yield a CBV-SNR only 9% and 12% worse, respectively, than that provided by infinite baseline points. $N_b > 50$ therefore seems to be a reasonable protocol before injection of agent to effectively minimize the noise from baseline estimation. As N_b increases, so too does the number of images acquired during a first-pass study, which often is limited by hardware constraints. However, for typical injections, the duration of the first-pass signal drop is approximately 20 seconds. Even with $N_b = 60$ and for the relatively short TR ≈ 1 second needed to maximize CBV-SNR with respect to TR, the complete first pass can be acquired well within 120 images, as illustrated in Figure 1a.

Figure 2b also suggests that the improvement in CBV-SNR gained by incorporating many baseline points is still realized even at very high input SNR. Therefore, large N_b is beneficial, even if σ_0 is small or S_0 is large, although in such cases, the fractional improvement in SNR due to increasing N_b will not be as great.

In Equations [7] and [13], the dependence of CBV-SNR on ζ has implications for the selection of N_b for various contrast agents. Contrast agents with greater molar relaxivity than Gd-DTPA (such as Dy-DTPA or iron oxide compounds) will yield a greater signal drop per dose of contrast agent. For these agents, the N_b required to achieve a particular SNR will decrease because ζ (a function of the shape of the signal drop) increases with percent signal drop and will outweigh the N_b term in Equation [7].

The results illustrated in Figure 3 demonstrate that we should opt for as large a percentage signal drop (large dose of contrast agent) as possible, because we can choose an appropriate TE to maximize CBV-SNR. As the dose and subsequent signal drop increases, CBV-SNR

peaks at a shorter TE, which is essentially a weighted average between the baseline T2 and the effective T2 at each time point during bolus passage. The larger the dose, the more the optimum TE falls below baseline T2. Nonetheless, CBV-SNR is relatively insensitive to TE around the optimum value even for doses of contrast agent yielding 70% signal drops. With the exception of very large signal drops (eg, 90% in Fig. 3), it is clear that for typical contrast agents, choosing TE equal to baseline T2 will provide nearly optimal results. For larger percentage signal drops, CBV-SNR drops more precipitously with increasing TE, suggesting that the appropriate choice of TE is more critical in these circumstances.

Figure 4a demonstrates that an optimal TR exists for spin-echo SNR. For very short TR, the reduced image SNR overwhelms the SNR improvement due to increased temporal resolution for the integration. For longer TR, there are simply too few points across the bolus to adequately estimate the area, and CBV-SNR diminishes. The effects of sample offset variation, included in the Monte Carlo numeric simulation, further reduce CBV-SNR with increasing TR for TR exceeding 1 to 2 seconds. For sufficiently large TR and concomitant coarse sampling of $\Delta R2(t)$, the numeric integration techniques yield a broader distribution of CBV. Variation in sampling times is particularly relevant either for tissue responses of short duration, for which a minimum TR is imposed, or for data sets with relatively high SNR, for which the variance due to integration scheme error predominates. The analytic and Γ -fit simulation results agree and exclude sample offset effects.

The analysis of optimal TR ignores the dependence of TE on TR. As TR approaches zero, TE must also approach zero. This has little effect on the spin-echo results for which peak SNR is attained with $TR \approx 1.25 T1$. For gradient-echo acquisitions with a TE optimally chosen for a given dose and expected peak signal change, SNR improves with decreasing TR and images should be acquired with the shortest TR that is permitted.

Figure 5 suggests that we should use as short an input bolus as possible. For a given TE, TR, and dose of contrast agent, as the bolus duration decreases, S_0/S_{min} increases and both the transit time and N decrease. As long as $\Delta R2(t)$ can be reconstructed (ie, sampling is not too coarse), the increase in S_0/S_{min} decreases the noise in measurement of V and therefore increases CBV-SNR. In Figure 5, the Monte Carlo results agree with the analytic model for sufficiently large input bolus duration (tissue response $MTT > 5$ seconds). The decrease in Monte Carlo CBV-SNR for short tissue response MTT reflects the inability of the numeric integration scheme to precisely integrate $\Delta R2(t)$ when the input time is unknown. This effect becomes increasingly more pronounced with increasing TR, because $\Delta R2(t)$ is more coarsely sampled. Monte Carlo studies using Γ -variate fits to estimate CBV suffer much less from this effect and agreed well with the analytic results (comparison not shown).

The results illustrated in Figure 6 suggest that a trade-off exists between CBV-SNR and the accuracy of relative CBV estimates. In the presence of recirculation or for vessels that are permeable to contrast agent (eg, leaky tumors), $\Delta R2(t)$ may not uniformly reflect CBV. A Γ -variate fit to $\Delta R2(t)$ may yield more accurate estimates of CBV, but these estimates may be less precise than those made with numeric integration. On the other hand, the Γ -variate correction for recirculation is, by its nature, an approximation; therefore, a complete numeric integration over a time scale that is long compared with the transit times is likely to be more accurate as well.

We note finally that there is a fundamental methodologic difficulty in verifying our semianalytic model describing CBV-SNR for a single voxel over multiple repetitions of the same experiment. Proper verification of our estimates would require multiple injections in each subject. Practical obstacles to obtaining such data make rigorous verification of the model difficult. Our approach in this study was to minimize the natural variation in CBV that occurs within an ROI by estimating CBV-SNR with the average standard deviation of CBV within small (2- and 4-pixel) sub-ROIs comprising a larger gray or white matter ROI.

It is worth mentioning the scaling factor used to account for the correlation introduced by the sub-ROIs. In our study, $S(t)$ had been smoothed in space with a Hanning filter (a normalized 3×3 matrix with rows $\{1/16 \ 2/16 \ 1/16\}$, $\{2/16 \ 4/16 \ 2/16\}$, and $\{1/16 \ 2/16 \ 1/16\}$), reflecting the way we typically process our CBV maps. The noise characteristics of σ_v (ie, $SNR_v \approx 84$) were thus of these Hanning-filtered data. The 2- and 4-pixel estimates of experimental σ_v were scaled by a factor accounting for the correlation introduced by the size of the sub-ROI to make a fair comparison between experimental σ_v and analytic σ_v .

The comparison summarized in Table 1 shows that predicted noise does not account for the total experimental noise, although the analytic σ_v from the 2-pixel sub-ROI for white matter accounts for 70% of the experimental CBV map noise. There are several explanations for the discrepancy. Biologic heterogeneity of CBV within the white and gray matter ROIs increases experimental σ_v but is not accounted for in the model. In essence, our experimental design assumes that the distribution of CBV values within the sub-ROIs is identical to that which would be obtained by repeated measurement of CBV within a single pixel. For this to be the case, the sub-ROIs would have to contain voxels with identical blood volume and biophysical parameters, including vessel size distribution, and the variation of contrast agent arrival times and concentrations would have to mimic those that occur on multiple injections for a single pixel. The contrast mechanism yielding $\Delta R2$ upon which our CBV maps are based is complicated and is a function of many biophysical variables, including volume fraction, vessel size and distribution, diffusion coefficient, contrast agent concentration, and vessel permeability, among others. (16) Therefore, tissues with identical blood volume may not necessarily have the same signal, and this can lead to variability in CBV estimates. In addition, the experimental σ_v reflects local tissue heterogeneity as well as true stochastic noise. It also is possible that temporal variation exists, perhaps due to biologic effects of contrast agent passage, which adds noise beyond that modeled by ζ .

The analytic σ_v is closer to experimental σ_v for white matter than it is for gray matter. Because gray matter ROIs contain much more contamination from cerebral spinal fluid, they are more heterogeneous than white matter ROIs and are expected to have more variation in CBV. Furthermore, analytic σ_v is closer to experimental σ_v for the 2-pixel sub-ROI than for the 4-pixel sub-ROI. There also is presumably less biologic heterogeneity within the 2-pixel sub-ROI than within the 4-pixel sub-ROI. The best we can do without replicating the injection in the same patient is two neighboring pixels, because it is more likely that biologic differences will be minimal (more similar true CBV, distribution of vessel sizes, delivery of contrast agent, etc.). However, like comparable estimates of the reproducibility of nuclear quantification techniques, the data imply that biologic heterogeneity

ultimately dictates the uniformity of computed CBV maps.

● **CONCLUSIONS**

We have quantified herein the main sources of noise in computed CBV maps. Through propagation of errors, we produced a semianalytic model for CBV map noise that has two terms: one due specifically to the variance of the integrated images, and one due to the estimate of the baseline. We introduced analytic and Monte Carlo techniques for determining the effect of experimental parameters and processing strategies on CBV-SNR. CBV-SNR increases as more points are used to estimate the baseline signal level. For typical injections, maps made with 10 baseline points have 34% more noise than those made with 50 baseline points. For a given peak signal drop and a particular shape of $\Delta R_2(t)$, we can choose a TE that maximizes CBV-SNR, and in general, this TE is less than the baseline T2. However, because CBV-SNR is relatively insensitive to TE around this optimum value, choosing $TE \approx T2$ does not sacrifice much SNR for typical doses of contrast agent. The TR that maximizes spin-echo CBV-SNR satisfies $TR/T1 \approx 1.26$, and as short a TR as possible should be used to maximize gradient-echo CBV-SNR. For physiologic input bolus durations at the optimum TE, CBV-SNR can be maximized for a given dose of contrast agent by selecting as short an input bolus duration as possible. For image SNR exceeding 20 to 30, the Γ -fitting procedure adds little extra noise compared with simple numeric integration. However, for noisier input images, as can be the case for high resolution echo-planar images, the covarying parameters of the Γ -variante fit broaden the distribution of the CBV estimate and thereby decrease CBV-SNR. We used the standard deviation of CBV within white and gray matter ROIs to estimate the noise in CBV maps constructed from actual patient data. Our analytic model accounts for roughly 70% of the measured variability of CBV within white matter ROIs, and the residual noise probably is attributed to biologic heterogeneity, sampling effects, and physiologic noise not included in the model.

● **Appendix**

This appendix derives the scaling factors that account for the correlation introduced by spatial filtering in the 2- and 4-pixel sub-ROIs used to estimate the experimental variance of V . We relate σ_v^2 , the experimental estimate of the variance of V , to σ_v^2 , the analytic estimate of the variance of V : $\sigma_v^2 = k\sigma_v^2$. We do this by deriving $\sigma_v^2 = a\sigma^2$ and $\sigma_v^2 = b\sigma^2$, where σ^2 is the baseline variance of the unfiltered image data, and solving $k = a/b$. As an example, we derive k for the 2-pixel sub-ROI.

a: Accounting for Spatial Correlation from the Hanning Filter

Because Hanning-filtered data are a linear combination of the original data, it follows that:

$$\sigma_v^2 = \sigma^2 \sum_{i=1}^9 c_i^2, \tag{A1}$$

where c_i are the (normalized) coefficients for the 3×3 Hanning filter:

$$\frac{1}{16} \begin{bmatrix} 1 & 2 & 1 \\ 2 & 4 & 2 \\ 1 & 2 & 1 \end{bmatrix}.$$

Therefore, $\sigma_v^2 = 9/64 \sigma^2$, and $a = 9/64$.

b: Accounting for Spatial Correlation from Sub-ROI Averaging

We consider a 2×1 sub-ROI in a CBV map, with a corresponding 4×3 grid of pixels $A \dots L$:

| | | | |
|---|-------------|-------------|---|
| A | B | C | D |
| E | F (V_1) | G (V_2) | H |
| I | J | K | L |

for which:

$$\sigma_v^2 \equiv \frac{1}{2} [(V_1 - \bar{V})^2 + (V_2 - \bar{V})^2] = \frac{1}{4} (V_1 - V_2)^2, \tag{A2}$$

where V_1 and V_2 are the estimated CBVs in the sub-ROI and \bar{V} is their mean. Because V_1 and V_2 are linear combinations of the unfiltered data (pixels $A \dots L$) with baseline noise σ^2 , the expectation of σ_v^2 , $E\{\sigma_v^2\}$, can be expressed in terms of F , G , and σ^2 :

$$E\{\sigma_v^2\} = E\left\{\frac{1}{4} (V_1 - V_2)^2\right\} = E\left\{\frac{1}{4} (F - G)^2\right\}, \tag{A3}$$

with

$$F = 1/16 \{A + 2B + C + 2E + 4F + 2G + I + 2J + K\} \tag{A4}$$

$$G = 1/16 \{B + 2C + D + 2F + 4G + 2H + J + 2K + L\} \tag{A5}$$

and

$$F - G = 1/16 \{A + B - C - D + 2E + 2F - 4G - 2H + I + J - 2K - L\}. \tag{A6}$$

Assuming that the unfiltered data ($A \dots L$) are uncorrelated, $E\{(F - G)^2\}$ is simply the sum of the expectation of the square of each term in Equation [A6], because the expectation of the product of cross-terms is equal to zero. Neglecting the mean, the expectation of the square of each term in Equation [A6] is proportional to σ^2 , and therefore, $E\{\sigma_v^2\} = 3/128 \sigma^2$, and $b = 3/128$.

Dividing a by b yields $k = 6$, and therefore, $\sqrt{k} = 2.45$ is used to scale the experimental estimate of σ_v for comparison with the analytic estimate of σ_v .

An analogous procedure was used to derive k for the 2×2 sub-ROI.

Acknowledgments: The authors thank Hannu Aronen, MD for acquiring the clinical data.

References

- Villringer A, Rosen BR, Belliveau JW, et al. Dynamic imaging with lanthanide chelates in normal brain: contrast due to magnetic susceptibility effects. *Magn Reson Med* 1988; 6:164-174.
- Rosen BR, Belliveau JW, Aronen HJ, et al. Susceptibility contrast imaging of cerebral blood volume: human experience. *Magn Reson Med* 1991; 22:293-299.
- Warach S, Li W, Ronthal M, Edelman RR. Acute cerebral ischemia: evaluation with dynamic contrast-enhanced MR imaging and MR angiography. *Radiology* 1992; 182:41-47.
- Sorensen AG, Kulke SM, Weisskoff RM, Boxerman JL, Buchbinder BR, Rosen BR. Investigation of cerebral hemodynamics with spirodiumide (Dy-DTPA-BMA) and functional magnetic resonance imaging (abstract). In: Book of abstracts: American Society of Neuroradiology 1994. Nashville, TN: American Society of Neuroradiology, 1994; 237.
- Belliveau JW, Kennedy DN, McKinstry RC, et al. Functional mapping of the human visual cortex using magnetic resonance imaging. *Science* 1991; 254:716-719.
- Zigun JR, Frank JA, Barrios FA, et al. Measurement of brain activity with bolus administration of contrast agent and gradient-echo MR imaging. *Radiology* 1993; 186:353-356.
- Frank JA, Mattay VS, Duyn J, et al. Measurement of relative cerebral blood volume changes with visual stimulation by 'double-dose' gadopentetate-dimeglumine-enhanced dynamic magnetic resonance imaging. *Invest Radiol* 1994; 29:S157-S160.

8. Gückel F, Brix G, Rempp K, Deimling M, Röther J, Georgi M. Assessment of cerebral blood volume with dynamic susceptibility contrast enhanced gradient echo imaging. *J Comput Assist Tomogr* 1994; 18:344-351.
9. Aronen HJ, Gazit IE, Pardo FS, et al. Multislice MRI CBV imaging of brain tumors: a comparison with PET studies (abstract). In: *Book of abstracts: Society of Magnetic Resonance in Medicine* 1993. New York: Society of Magnetic Resonance in Medicine, 1993; 485.
10. Aronen HJ, Gazit IE, Louis DN, et al. Cerebral blood volume maps of gliomas: comparison with tumor grade and histologic findings. *Radiology* 1994; 191:41-51.
11. Maeda M, Itoh S, Kimura H, et al. Tumor vascularity in the brain: evaluation with dynamic susceptibility-contrast MR imaging. *Radiology* 1993; 189:233-238.
12. Thompson HK, Starmer CF, Whalen RE, McIntosh HD. Indicator transit time considered as a gamma variate. *Circ Res* 1964; 14:502-515.
13. Starmer CF, Clark DO. Computer computations of cardiac output using the gamma function. *J Appl Physiol* 1970; 28:219-220.
14. Lassen NA, Perl W. *Tracer kinetic methods in medical physiology*. New York: Raven Press, 1979.
15. Weisskoff RM, Belliveau J, Kwong K, Rosen B. Functional MR imaging of capillary hemodynamics. In: Potchen EJ, Haacke EM, Siebert JE, Gottschalk A, eds. *Magnetic resonance angiography: concepts and applications*. St. Louis: CV Mosby, 1992; 473-484.
16. Boxerman JL, Hamberg LM, Rosen BR, Weisskoff RM. MR contrast due to intravascular magnetic susceptibility perturbations. *Magn Reson Med* 1995; 34:555-566.
17. Belliveau JW, Cohen MS, Weisskoff RM, Buchbinder BR, Rosen BR. Functional studies of the human brain using high-speed magnetic resonance imaging. *J Neuroimaging* 1991; 1:36-41.
18. Press WH, Flanner BP, Teukolsky SA, Vetterling WT. *Numerical recipes in C: the art of scientific computing*. New York: Cambridge University Press, 1988.
19. Bevington PR, Robinson DK. *Data reduction and error analysis for the physical sciences*. New York: McGraw-Hill, 1992.
20. Boxerman JL, Weisskoff RM, Aronen HJ, Rosen BR. Signal-to-noise and tissue blood volume maps from dynamic NMR imaging studies (abstract). In: *Book of abstracts: Society of Magnetic Resonance in Medicine* 1992. Berlin: Society of Magnetic Resonance in Medicine, 1992; 1130.
21. Allan DW. Time and frequency (time-domain) characterization, estimation, and prediction of precision clocks and oscillators. *IEEE Trans Ultrasonics Ferroelec Freq Control* 1987; UFFC-34: 654-657.
22. Bahn MM. A single-step method for estimation of local cerebral blood volume from susceptibility contrast MRI images. *Magn Reson Med* 1995; 33:309-317.